Vacuum 123 (2016) 151–159

Contents lists available at ScienceDirect

Vacuum

journal homepage: www.elsevier.com/locate/vacuum

Investigation of the thickness effect on material and surface texturing properties of sputtered ZnO:Al films for thin-film Si solar cell applications

Xia Yan [a, b], Weimin Li [a, c], Armin G. Aberle [a, b, c], Selvaraj Venkataraj [a, *]

[a] Solar Energy Research Institute of Singapore, National University of Singapore, 7 Engineering Drive 1, 117574 Singapore, Singapore
[b] NUS Graduate School for Integrative Sciences and Engineering (NGS), National University of Singapore, 28 Medical Drive, 117456 Singapore, Singapore
[c] Department of Electrical and Computer Engineering, National University of Singapore, 4 Engineering Drive 3, 117576 Singapore, Singapore

ARTICLE INFO

Article history:
Received 18 August 2015
Received in revised form
24 October 2015
Accepted 26 October 2015
Available online 30 October 2015

Keywords:
ZnO:Al
Film thickness
Magnetron sputtering
Surface texturing
Thin film

ABSTRACT

Transparent conductive Al-doped ZnO (AZO) layers are widely used as the front electrode for thin-film silicon solar cells. For superstrate configurations, the front AZO layer simultaneously provides both electrical conductance and optical scattering. To improve the device performance, a textured surface is needed to enhance the photogeneration inside the solar cell through better light scattering. One approach is to wet-chemically etch the AZO films using hydrochloric (HCl) acid. In this work, AZO films with different initial layer thicknesses (900, 700 and 500 nm) are deposited onto soda-lime glass via magnetron sputtering and their texturing behaviours are compared. It is found that not only the material properties but also the surface texturing process greatly depends on the as-grown thickness of the AZO layer. The increased resistivity is mainly caused by a deteriorating carrier mobility as the thickness reduces. In terms of morphology, thick AZO films (i.e., 900 and 700 nm) show similar texture features after etching. In contrast, the thin AZO films (i.e., 500 nm) show irregularly shaped textures and over-etching, which leads to limited scattering. Hence the AZO layer thickness must be suitably chosen to achieve both good electrical conductance and optical scattering for high-efficiency thin-film Si solar cell applications.

1. Introduction

Transparent conductive oxide (TCO) materials have been widely used as the front electrode for thin-film silicon (Si) solar cells [1–3]. Common TCOs include aluminium-doped zinc oxide (ZnO:Al or AZO), tin-doped indium oxide (In_2O_3:Sn or ITO) and fluorine-doped tin oxide (SnO:F or FTO) [4]. Of these, sputter-deposited AZO is becoming more favoured as the front electrode owing to its advantages such as stability against a hydrogen plasma, abundance of materials, low cost and easy post-deposition texturing for light trapping [5–7]. Compared with the market dominating ITO, the properties of AZO films depend more strongly on the as-grown layer thickness, especially the electrical performance. The literature shows that the AZO layer should be at least about 600 nm thick in order to obtain good carrier mobility and thus a low resistivity of the order of 10^{-4} Ωcm [8,9].

For thin-film Si solar cells prepared in a superstrate (p-i-n) configuration, the sheet resistance (R_{sh}) of the front TCO electrode should be less than 10 Ω/sq to avoid excessive ohmic losses [10]. Thus, even for a highly conductive AZO layer with a resistivity of 6×10^{-4} Ωcm, this application requires an AZO thickness of at least 600 nm to meet the electrical requirement. This basically excludes the use of thin AZO films for thin-film Si solar cells applications, from a purely electrical point of view.

In addition to electrical requirements, the front AZO layer also functions as the optical layer of the solar cells. To achieve better device performance, the AZO layer needs a rough surface texture to effectively scatter incident light inside the solar cell. An efficient scattering scheme prolongs the optical pathlength and thus leads to enhanced photon absorption within the absorber layer [11]. For sputter-deposited AZO films, one common approach is to wet-chemically etch the films in weak or diluted acids, such as hydrochloric (HCl) acid [12–15].

It is well known that the deposition techniques and conditions can greatly affect the resultant film properties. But in addition to the process parameters, the layer thickness can also play a major

* Corresponding author.
E-mail address: s.venkataraj@nus.edu.sg (S. Venkataraj).

http://dx.doi.org/10.1016/j.vacuum.2015.10.027
0042-207X/

role in determining the electrical, optical, structural and annealing properties of AZO films [16–21]. O. Madani Ghahfarokhi et al. showed that the strong dependence of the resistivity on the layer thickness is related to the formation of larger grains in a thicker film for DC-sputtered AZO films [21]. However, only a few studies were carried out to understand the thickness effect and surface texturing properties of AZO films, especially for thin-film Si solar cell applications. W. Böttler et al. analysed the relationship between lateral and vertical dimensions of crater-like textures of RF-sputtered ZnO films with as-deposited thickness and etching time [22], while V. Smirnov et al. further investigated the surface morphology variations after HCl texturing, focused on ZnO/Ag back reflectors applied for thin-film microcrystalline Si (μc-Si:H) solar cells prepared in a substrate (n-i-p) configuration [23].

Therefore, in this work we not only systematically investigate the film thickness effect on the material properties of the AZO layer, but also focus on the surface texturing process with regard to its electrical conductance, optical scattering and morphological properties. AZO films with different initial layer thicknesses were deposited onto planar soda-lime glass substrates by pulsed DC magnetron sputtering. We found that the texturing properties also greatly depend on the as-grown AZO film thickness. The AZO layer must have a minimum initial thickness to be able to accommodate the thickness reduction during the texturing process, which is required to achieve well-etched surface textures and thus a high haze value. Their limited optical scattering capability excludes the use of thin AZO films (<500 nm initial thickness), from the optical point of view, as the front electrode for superstrate thin-film Si solar cell applications.

2. Experimental details

2.1. Sample preparation

In this study, AZO films with three different as-grown layer thicknesses (900, 700 and 500 nm) were deposited on A3 size (40 cm × 30 cm, 3 mm thick) planar soda-lime glass sheets at identical deposition conditions by magnetron sputtering. Dual cylindrical rotatable magnetron ZnO:Al_2O_3 (98:2 wt%) sputter targets were used to deposit AZO films in an inline multi-chamber sputter machine (FHR Anlagenbau, model Line540). During deposition, the heater temperature was kept constant at 375 °C (the corresponding substrate temperature was estimated to be about 200 ± 5 °C). Pure argon and oxygen-diluted argon (99% Ar and 1% O_2) were introduced into the chamber as processing gases at a constant flow rate of 155 and 50 sccm, respectively. The overall oxygen content was around 0.24%. The corresponding working pressure in the chamber was maintained at approximately 3×10^{-3} mbar. The sputter system was operated in the pulsed DC mode, with an applied power of 2 kW on each cathode. The deposition was carried out in the dynamic mode (i.e., multiple pass deposition). The glass sheet was vertically attached (i.e., portrait format) on a moving carrier and allowed to oscillate in front of the cathodes at a constant speed of 15 mm/s for 18, 14 or 10 times, in order to reach a film thickness of either 900, 700 or 500 nm. The deposition rate was around 50 nm/pass. It should be noted that the deposition parameters (DC or RF sputtering, chamber pressure and substrate temperature) of the AZO films could significantly affect the following etching behaviour, which can be well described by a modified Thornton model proposed by O. Kluth et al. in Ref. [24]. A higher deposition pressure would result in an increased etching rate while the texture-etched morphology changes from crater-like to hill-like appearance. In this work, the deposition condition was tuned to a trade-off condition with both good film properties and texturing-friendly. The deposition conditions and some of the resulting AZO film properties are summarised in Table 1.

2.2. Characterisation

A double-beam UV/Vis/NIR spectrophotometer (Agilent, Cary 7000) with an integrating sphere was employed to characterise the optical properties of the AZO films before and after the surface texturing step. Both total and diffuse transmittance spectra into air were recorded. The transmission haze is utilised to distinguish the optical light scattering properties of various surface morphologies resulting from texturing the AZO films [25,26], as calculated via:

$$Haze\ (\%) = \frac{T_{diff}}{T_{total}} \times 100\% \quad (1)$$

where *Haze*, T_{diff} and T_{total} are the transmission haze, the diffuse transmittance and the total transmittance. The haze value at 600 nm wavelength is taken for the comparisons in Sect. 3.2, since the intensity of the solar spectrum (AM 1.5G) peaks near this wavelength [27].

The electrical properties of the AZO films were measured by the van der Pauw method in a Hall measurement system (Bio-Rad/Accent, HL5500). In order to avoid high free carrier absorption, it is desirable to achieve low electrical resistivity via a high carrier mobility. The film resistivity was calculated based on the obtained carrier mobility and concentration via:

$$\rho = \frac{1}{ne\mu_e} \quad (2)$$

where ρ is the film resistivity, n is the carrier concentration, e is the elementary charge and μ_e is the carrier mobility of the film.

The microstructures of these as-deposited AZO films were characterised by X-ray diffractometry (XRD; Bruker D8) and Raman spectroscopy (Renishaw, inVia Raman Microscope). The XRD measurements were carried out using a Cu K_α radiation source (λ = 1.5406 Å). The crystallite size of the films was calculated from the full width at half-maximum (FWHM) of the XRD pattern, using the Scherrer equation [28]:

$$D = \frac{K\lambda}{B\cos\theta_B} = \frac{0.9 \times 0.15406}{B\cos\theta_B} \quad (3)$$

where D is the crystallite size, K is the shape factor (which has a typical value of around 0.9), λ is the wavelength of the X-rays, B is the line breadth of FWHM in radian, and θ_B is the Bragg angle in degrees.

Scanning electron microscopy (SEM; Carl Zeiss, Auriga-39-35) and atomic force microscopy (AFM; Veeco, NanoScope D3100) were used to record the surface morphologies of the textured AZO films. During the SEM measurements the samples were tilted by 45° and the images were recorded with a magnification of 20,000. The AFM scan was taken in the central region of each sample in the tapping mode, at a constant tapping rate of 0.5 Hz. The AFM image area was set as 10 μm × 10 μm (each containing 512 × 512 data points). The AFM results were further processed with a self-programmed MATLAB code to statistically analyse the surface height and inclination angles of the textured AZO films. The root-mean-square (RMS) roughness value denotes how rough the textured surface is. Details on the AFM-MATLAB processing procedure can be found in Refs. [29–31].

3. Results and discussion

3.1. Thickness effect on material properties

The electrical performance of sputter-deposited AZO films is

Table 1
Deposition conditions and selected film properties of sputter-deposited AZO films with different layer thicknesses.

	Power (kW)	Ar (sccm)	1% O_2-diluted Ar (1 sccm)	O_2 content (%)	Pressure (mbar)
AZO (900 nm)	2.0	155	50	0.24	3×10^{-3}
AZO (700 nm)	2.0	155	50	0.24	3×10^{-3}
AZO (500 nm)	2.0	155	50	0.24	3×10^{-3}
	Heater temperature (°C)	Number of oscillation pass	Visible transmission (%)	Visible haze (%)	Sheet resistance (Ω/sq)
AZO (900 nm)	375	18	86.9	0.32	5.5
AZO (700 nm)	375	14	87.1	0.19	8.0
AZO (500 nm)	375	10	87.2	0.14	17.8

quite sensitive to the as-grown layer thickness, as shown in Fig. 1. The electrical properties significantly deteriorate for thin AZO films. The increased resistivity, from 5.2×10^{-4} to 9.3×10^{-4} Ωcm, is mainly caused by the deteriorating carrier mobility for thin films, which decreases greatly from 31.8 to 17.7 cm^2/V when the layer thickness reduces from 900 to 500 nm (see Fig. 1). At the same time, the carrier concentration stays almost constant, at about 3.7×10^{20} cm^{-3}. Therefore this deteriorating mobility is very likely caused by increased grain boundary scattering, due to reduced mean crystallite size of the thin films [32].

The sheet resistance is another commonly used value to quantify the lateral electrical conductance of AZO films, which correlates the film resistivity and the layer thickness. A value of 5.5 Ω/sq was obtained for 900 nm thick AZO films, 8.0 Ω/sq for 700 nm films, and 17.8 Ω/sq for 500 nm films, see Fig. 1. It should be noted that, as a rule of thumb, the sheet resistance value of the TCO layer should be less than 10 Ω/sq in order to provide sufficient electrical conductance as the front electrode of superstrate thin-film Si solar cells [10].

With regard to the film structure, polycrystalline ZnO films usually exhibit a preferred (002) orientation of the grains (*c*-axis orientation normal to the substrate surface), since the (002) plane has the lowest surface free energy [33,34]. Our XRD results of Fig. 2(a) confirm that these AZO films crystallise in a hexagonal wurtzite structure. Fig. 2(b) shows a magnified view of the XRD profiles of the (002) peak. It can clearly be seen that the film crystallinity deteriorates as the layer thickness decreases, as shown by the reduced (002) peak intensity at around $2\theta = 34.4°$. Simultaneously, the calculated crystallite size slightly decreases from 19.6 to 18.6 nm while the FWHM increases from 0.424° to 0.446°, see Fig. 2(c) and Table 2.

Fig. 3 shows the Raman patterns of these AZO films measured in the backscattering configuration. As a wurtzite structure, ZnO belongs to the space group C_{6v}^4 [35,36]. In this symmetry, the optical phonons at the Γ point of the Brillouin zone follow the irreducible representation:

$$\Gamma = A_1 + E_1 + 2B_1 + 2E_2 \quad (4)$$

where A_1 and E_1 modes are both polar and thus each split into transverse optical (A_1-TO and E_1-TO) and longitudinal optical modes (A_1-LO and E_1-LO), with different frequencies due to the macroscopic electric fields associated with the LO phonons. The A_1 and E_1 modes are both Raman and infrared active, while the B_1 modes are inactive (silent mode). In addition to LO and TO phonon modes, there are two non-polar Raman active phonon modes with

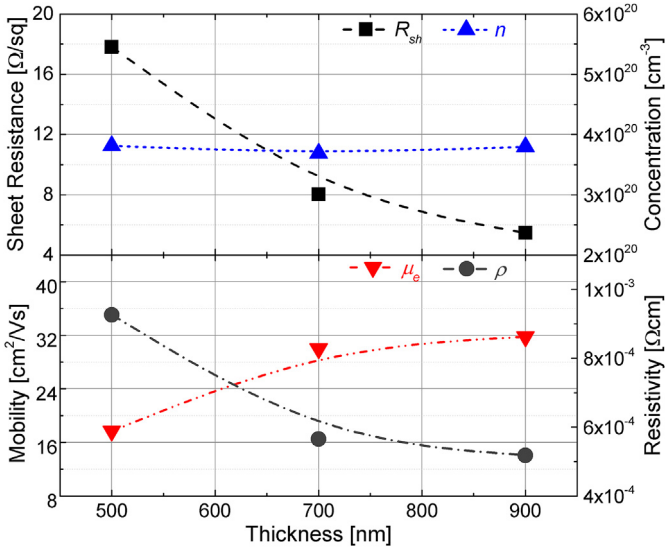

Fig. 1. Variation of sheet resistance and carrier concentration (top), Hall mobility and resistivity (bottom) of sputter-deposited AZO films as a function of as-grown layer thickness. The dashed lines are guides to the eye.

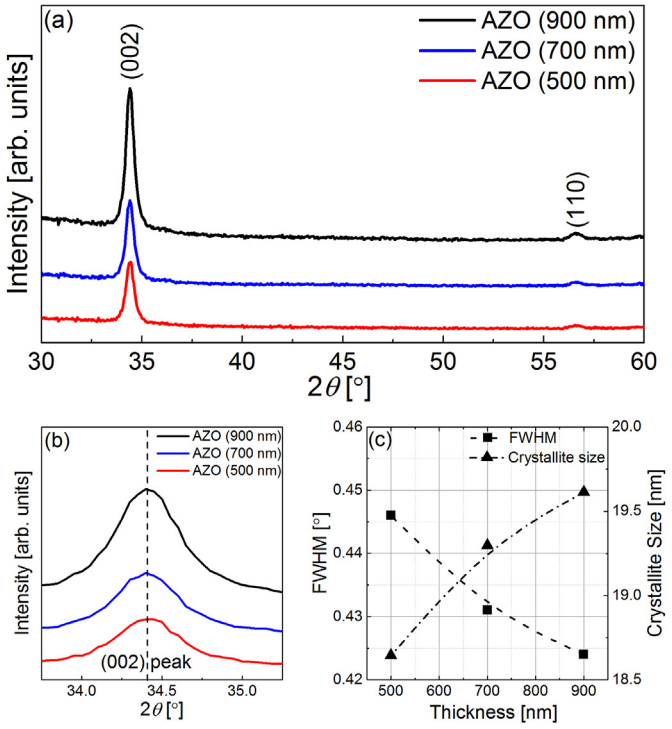

Fig. 2. (a) XRD profiles of as-deposited AZO films with layer thicknesses of 900, 700 and 500 nm. (b) Magnified view of plot (a) around the (002) peak. (c) Corresponding FWHM and crystallite size of the (002) peak.

Table 2
XRD and Raman results of as-deposited AZO films with different layer thicknesses.

		AZO (900 nm)	AZO (700 nm)	AZO (500 nm)
XRD	Peak	(002)	(002)	(002)
	2θ (°)	34.36	34.44	34.37
	FWHM (°)	0.424	0.431	0.446
	Crystallite size (nm)	19.6	19.3	18.6
Raman	Peak	A_1-LO	A_1-LO	A_1-LO
	Wavenumber (cm^{-1})	563.5	563.0	562.5
	FWHM (cm^{-1})	52.5	42.4	40.8

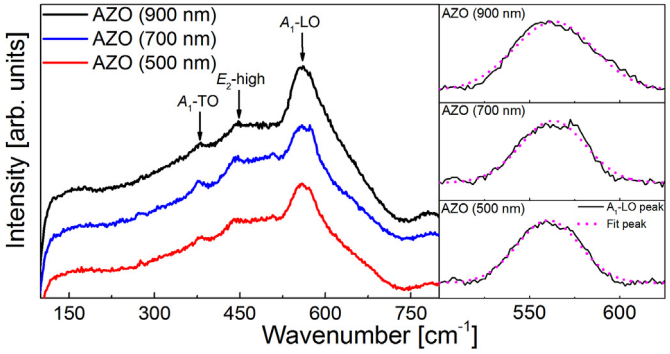

Fig. 3. Raman profiles of as-deposited AZO films with layer thicknesses of 900, 700 and 500 nm. The arrows indicate the positions of Raman peaks. The A_1-LO peak is fitted with a Gaussian profile.

symmetry E_2. The E_2 (low-frequency) mode is associated with the vibration of the heavy zinc sublattice, while the E_2 (high-frequency) mode involves only oxygen atoms [37]. Due to the selection rule and the non-Raman-active modes, only the A_1-LO and E_2 modes are expected to be observable when the incident light is normal to the sample surface [38].

The Raman results also reveal similar variations of the film structure. The Raman profile of AZO films is dominated by the A_1-LO vibration mode that appears as a symmetric peak at around 563 cm^{-1}, see Fig. 3. This primary A_1-LO peak can be well fitted with a Gaussian profile. As the film thickness decreases, the peak intensity of the A_1-LO vibration tends to decrease accordingly while the Raman shift peak only slightly changes by 1 cm^{-1}. It is known that the shift of the peak position can be attributed to residual stress, structural disorder and crystal defect in the films [35]. Approximately the same Raman shift peak indicates similar structural stress between these three AZO films with different layer thicknesses. The other two weak peaks can be attributed to the ZnO vibration modes of A_1-TO and E_2-high, respectively. The presence of the A_1-TO mode is related to the polycrystallinity of the films, although it is not expected for single crystalline ZnO [39]. The appearance of the E_2 mode suggests preferred wurtzite structure of the AZO grains [40], which agrees with the XRD observation shown in Fig. 2.

3.2. Thickness effect on the surface texturing properties

The literatures show that various acidic solutions and alkaline

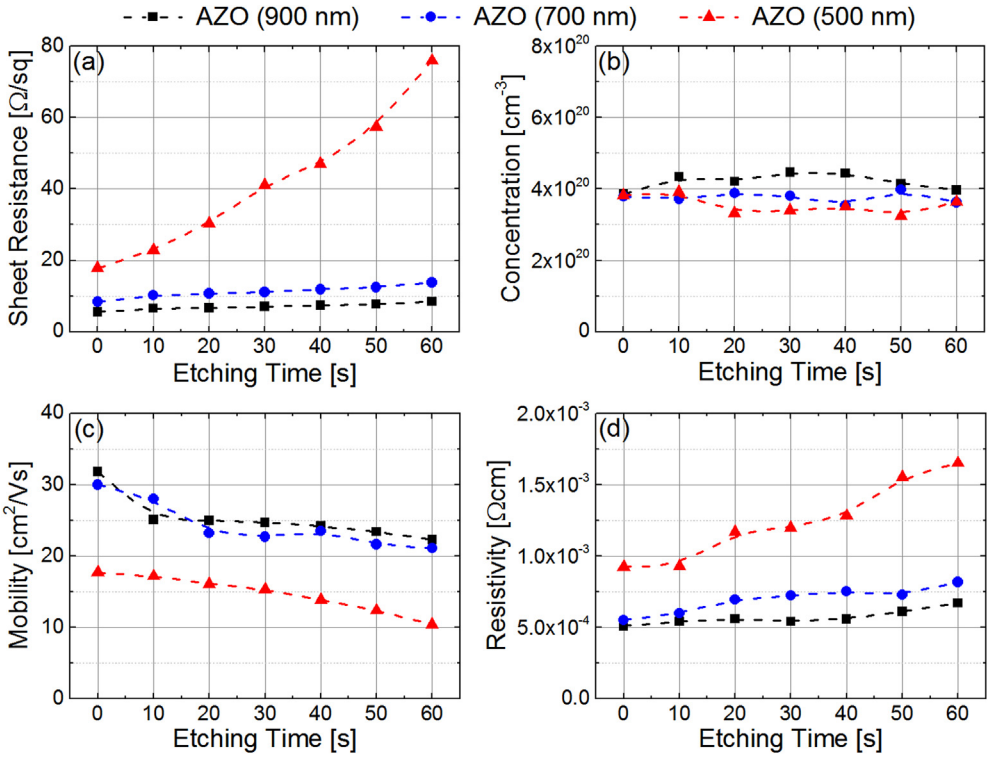

Fig. 4. Variation of (a) sheet resistance, (b) carrier concentration, (c) Hall mobility, and (d) resistivity as a function of the etching time of AZO films with different as-grown layer thicknesses. The values at 0 s denote the initial value of the as-deposited films. The dashed lines are guides to the eye.

etchants can be used for the post-deposition etching of AZO films, and the resultant surface morphologies can greatly depend on the etchants [41–43]. Among these etchants, the HCl-etched films typically produce good texture features and strong light scattering [44,45]. Therefore in this work, after deposition, the AZO films were wet-chemically textured by standard HCl etching to obtain rough surface texture features for the purpose of light scattering. To better control the etching process, the HCl acid was diluted with deionised (DI) water to a volume concentration of 0.5%. The surface morphology was modified accordingly by varying the HCl etching time. It was observed that the HCl etching gradually deteriorates the electrical properties of the AZO films. These AZO films show both increased sheet resistance value and film resistivity after the surface texturing, as shown in Fig. 4(a, d). The increased sheet resistance is not only due to the reduced film thickness, but also due to a reduced carrier mobility (see Fig. 4(c)). The mobility slightly decreases from 31.8 to 22.3 cm^2/V for the 900 nm AZO film, 30.0 to 21.1 cm^2/V for the 700 nm film, and 17.7 to 10.4 cm^2/V for the 500 nm film, when the etching time increases from 0 to 60 s. This reduced mobility was caused by the jagged surface textures, which could significantly affect the movement of carriers and thus deteriorate the electron conductance within the textured films. At the same time, the carrier concentration remains relatively constant at about 4×10^{20} cm^{-3} (see Fig. 4(b)). As a result, the sheet resistance of the 900 nm AZO films gradually increases from initially 5.5 to 8.4 Ω/sq, while the sheet resistance of the 700 nm films increases from 8.0 to 13.8 Ω/sq. In contrast, the sheet resistance of the 500 nm thick AZO film quickly rises to 76.0 Ω/sq after 1 min of etching, which more than quadruples the initial value of the as-grown film (17.8 Ω/sq). Such a high sheet resistance would cause severe ohmic losses in thin-film Si solar cell applications.

With regard to the optical properties, the AZO layer needs to be as transparent as possible. It is beneficial to have a high transmission (>80%) in the visible range. In addition, the textured surface helps to scatter light for an elongated light path and thus leads to an enhanced photogeneration in the solar cell. In this work, the

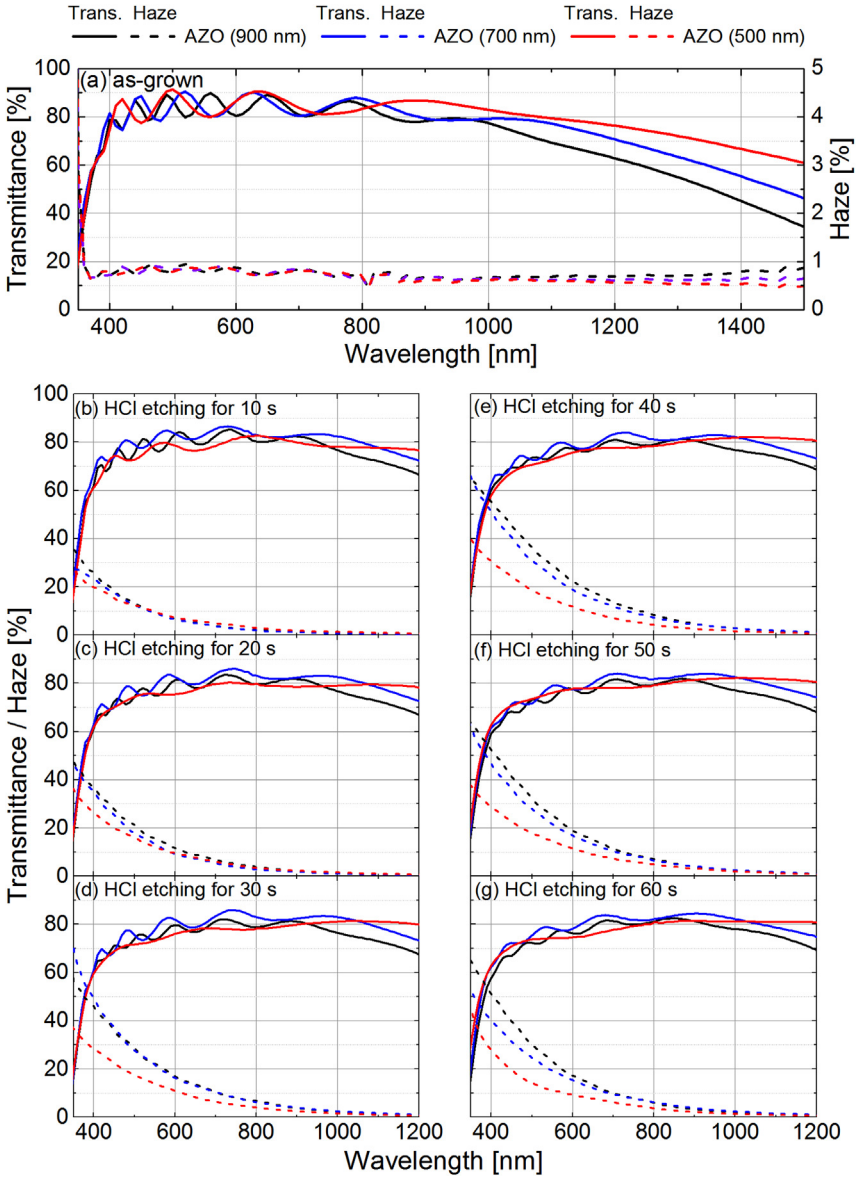

Fig. 5. Optical transmittance (solid lines) and haze (dashed lines) of AZO films with different as-grown layer thicknesses of 900, 700 and 500 nm, in the (a) as-grown state, and after HCl etching for (b) 10 s, (c) 20 s, (d) 30 s, (e) 40 s, (f) 50 s, and (g) 60 s.

haze value at 600 nm wavelength is used to represent the optical light scattering capability of the textured AZO films. The haze value is the ratio of the diffuse transmission of the sample and the total transmission, see Eq. (1). It should be noted that commercially available TCO substrates (e.g., the Asahi U-type TCO) usually have a haze value in the range of 15–20%.

Fig. 5(a) shows the transmittance and corresponding haze values of the as-deposited AZO films before the surface texturing step. The transmittance spectra have a thickness-dependent sinusoidal pattern of interference fringes. Due to a bandgap energy of ~3.4 eV, the AZO films become highly absorbing for ultraviolet (UV) light below 370 nm. In the visible range, the AZO films show a high transmission value of around 85%. In the near-infrared (NIR) range, the transmission starts to rapidly decrease beyond about 1000 nm wavelength (especially for the thicker films), which is caused by free carrier absorption. As can be seen from Fig. 5(a), these as-deposited AZO films have negligible scattering ability, with haze values of less than 1% across the entire solar spectrum.

Fig. 5(b–g) show the spectral transmittances and haze values after the surface texturisation step, for different etching durations. As the texturing proceeds from 10 to 60 s, the intensity of the interference fringes gradually reduces due to the roughening of the surface, and the overall visible transmission decreases slightly (by a few percent) for all samples. With regard to the optical haze, the resultant haze value of the textured AZO reduces for thin films (especially for the 500 nm film) for the same etch time. For all samples, the highest haze value was obtained after 40 s of HCl etching. The value (at 600 nm wavelength) is 22% for the 900 nm thick AZO film, 19% for the 700 nm film, but only 12% for the 500 nm film, see Fig. 5(e). In addition to the light scattering (haze), the rugged surface textures also provide the anti-reflective effects (graded index of refraction). The AZO film with lowest thickness has less good anti-reflection properties, and thus high reflection at the front side and slightly reduced transmittance compared to other two AZO films. It is important to note that the actual value of the haze and transmission into Si should be much higher than the value measured into air owing to a much high refractive index (n of ~4) of the thin-film Si material.

In addition to the exact value, the overall trend as a function of etching time also differs for the thin films. The haze of the 500 nm thick AZO film fluctuates around 10%, showing little improvement as the etching time increases from 10 to 60 s. In contrast, the haze value of the 700 nm and 900 nm thick films initially increases from less than 10% to around 20% when the etching time increases from 10 to 40 s, and then slightly decreases by 2–3% (i.e., etching for 50 or 60 s).

The SEM micrographs shown in Fig. 6 and the AFM 2D images shown in Fig. 7 compare the texture features of the AZO layers with different as-grown film thicknesses after HCl etching for 10, 30 and 50 s. All these texture-etched films show a porous surface covered by many small hole-like features (around 100–200 nm wide) together with large texture features (~1 μm wide). The large-sized textures are commonly observed as a result of the etching of (002) oriented c-axis grains [15,46], while the hole-like porous features are speculated to be caused by the etching of other oriented grains, such as (103) grains [47], or by surface defects.

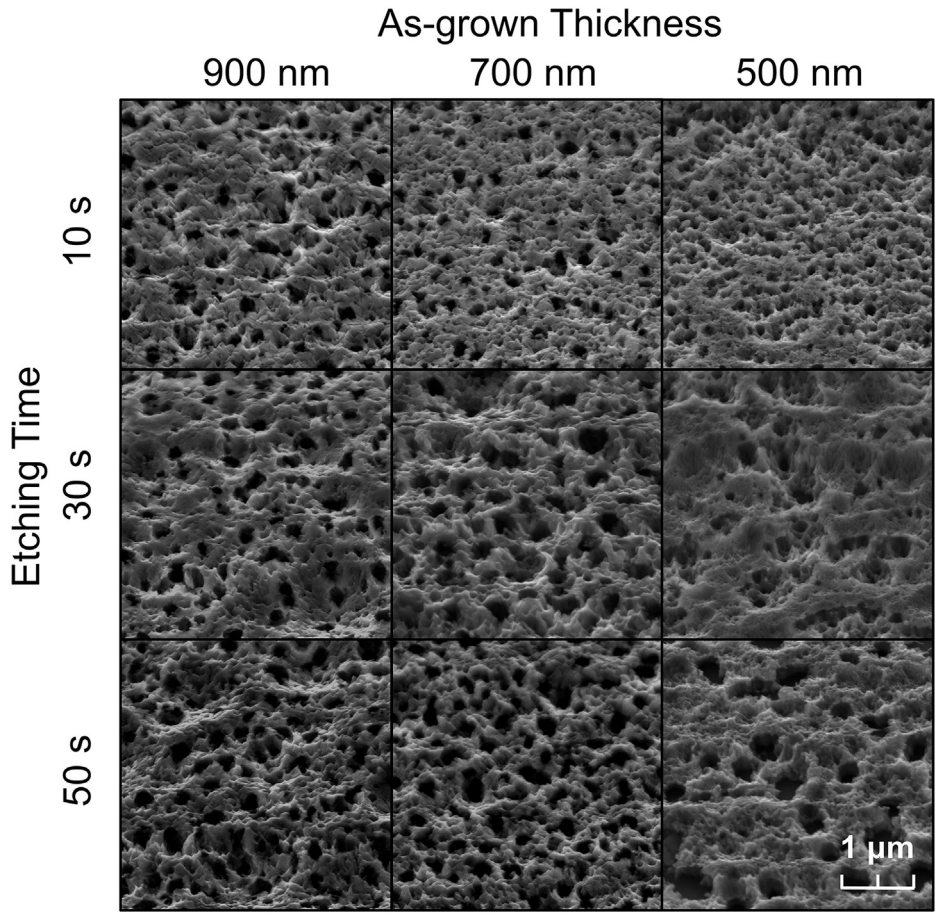

Fig. 6. SEM micrographs of surface textured AZO films with different as-grown layer thicknesses of 900, 700 and 500 nm, after HCl etching for 10, 30 and 50 s.

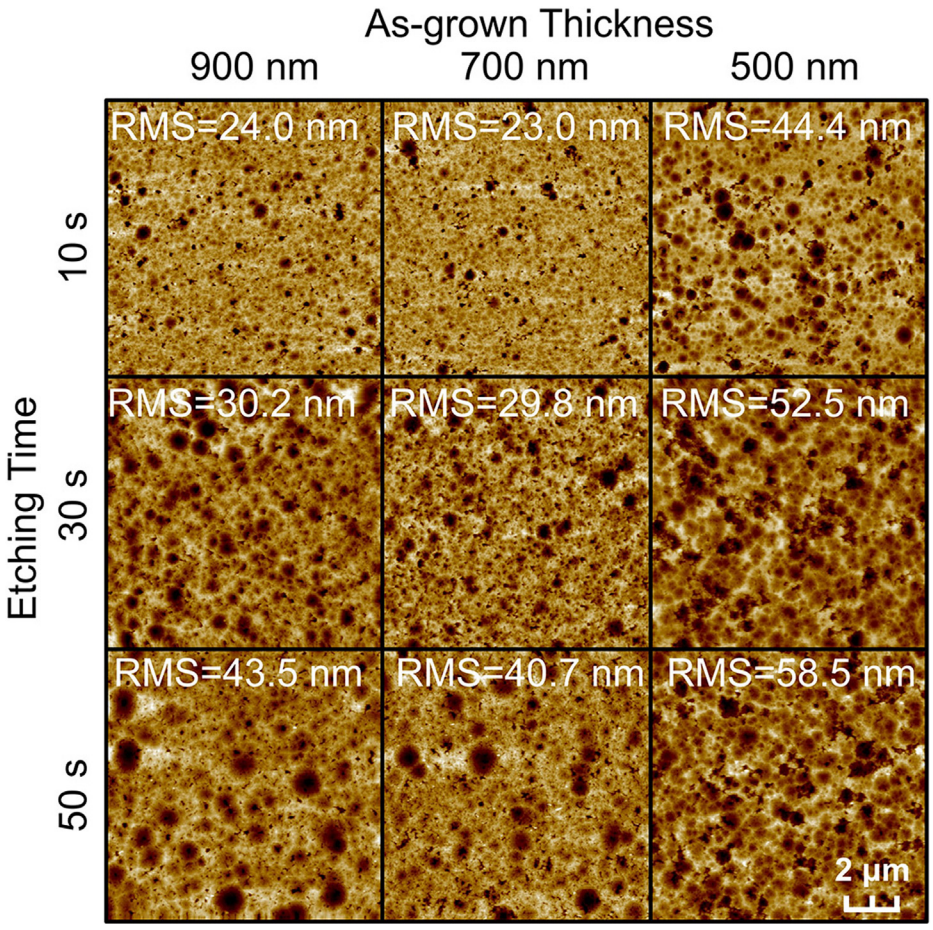

Fig. 7. AFM images of surface textured AZO films with different as-grown layer thicknesses of 900, 700 and 500 nm, after HCl etching for 10, 30 and 50 s. Also shown is the RMS roughness value of each sample.

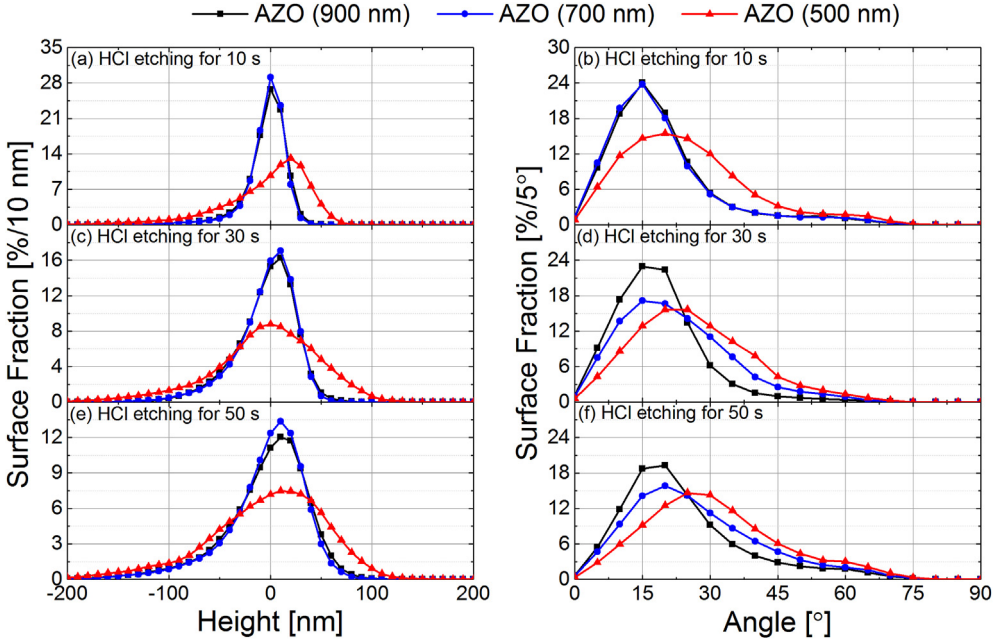

Fig. 8. (a, c, e) Surface height, and (b, d, f) angle distribution derived from AFM measurements of surface textured AZO films with different as-grown layer thicknesses of 900, 700, and 500 nm, after HCl etching for 10, 30 and 50 s.

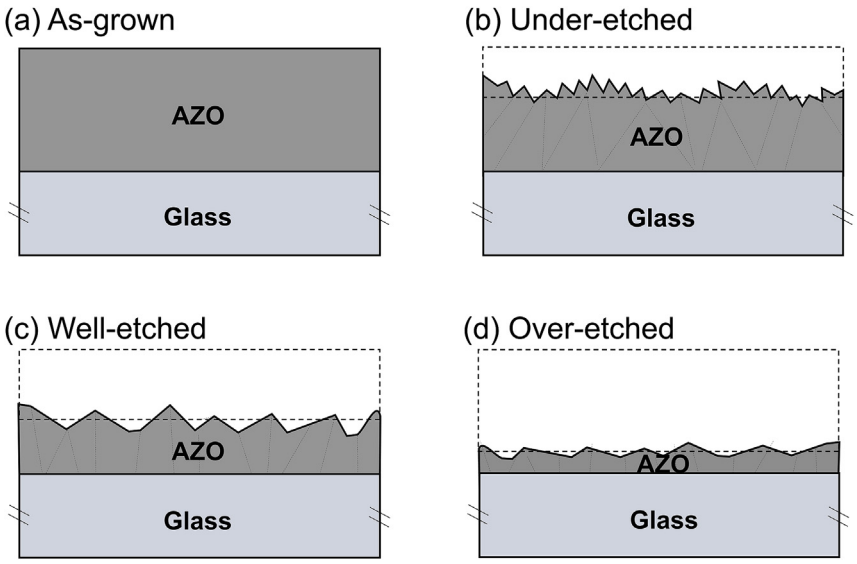

Fig. 9. Schematic diagram of sufficiently thick AZO films during the surface texturing process: in the states of (a) as-grown, (b) under-etched, (c) well-etched, and (d) over-etched. The dashed line indicates the thickness reduction caused by the HCl etching.

As shown in Figs. 6 and 7, the texture feature morphology differs between the thicker (900 and 700 nm) and the thinner (500 nm) AZO films, especially after HCl etching for at least 30 s. For the thick films, further etching laterally expands the texture feature size while inducing more hole-like texture features across the surface. These uniformly distributed texture features enhance the light scattering (i.e., give a higher haze value). By comparison, the textured surface of the thin AZO films is sparsely covered by much larger and deeper hole-like features (up to 400–500 nm wide and ~200 nm deep). Further etching to 50 s leads to complete film removal and an abrupt over-etched surface in certain areas, which greatly affects the electrical conductance while barely contributing to the optical scattering. Compared to commonly observed crater-like structures [48–50], the hole-like textures obtained in this work have a small average lateral feature size and thus low scattering capabilities for long-wavelength light. As a result, this type of morphology may not be good for μc-Si:H solar cells which require effectively optical enhancement in the NIR region. While for amorphous Si (a-Si:H) based solar cells, due to bandgap limitations the device is able to absorb photons only up to ~800 nm and long-wavelength scattering makes no more difference. In addition, the obtained texture morphology has lower surface roughness compared to that of the crater-like structures, which helps to reduce the shunting issues and thus beneficial for the fabrication of thin-film solar diodes.

Statistical analysis of the AFM data enables a direct comparison of the obtained surface morphologies of these HCl-textured AZO films [29–31]. Fig. 8 shows the distribution histograms of the surface height (in 10-nm increments) and the inclination angle (in 5-degree increments). Of these textured films, the AZO film with an as-grown thickness of 500 nm shows the broadest distributions of both height and angle. The angle distribution peaks at about 25°, approximately 10° higher than that of the thick films. Such a broad distribution is correlated with these over-etched surface textures, which result in a higher surface roughness value. In contrast, it can be seen that the 900 and 700 nm thick films have similar height and angle distributions after etching. As expected, these two films have similar surface roughness. Further etching from 10 to 50 s gradually broadens the distribution and roughens the surface, which correlates well with the morphology variations observed by SEM and AFM (see Figs. 6 and 7).

In summary, the surface texturing process of sufficiently thick AZO films can be separated into four stages, as shown in Fig. 9. The as-grown state refers to as-deposited films by magnetron sputtering without any surface texturing treatments. After HCl etching for 10–20 s, the AZO films are under-etched with a few small-sized texture features distributed over the surface. Etching for 30–40 s typically gives a well-etched surface covered by large texture features, and thus capable of strong light scattering. Longer etching for 50 s and above leads to an over-etched surface, which deteriorates the texture morphology and thus leads to a reduced haze value. In contrast, for thin AZO films there are hardly any well-etched surface textures observed. The resultant morphology directly transits from the under-etched to the over-etched stage as the etching proceeds, since there is an insufficient amount of film to accommodate the thickness reduction during the formation of large texture features.

4. Conclusion

In this work, three AZO films with different as-grown layer thicknesses (900, 700 and 500 nm) were prepared on planar soda-lime glass sheets by pulsed DC magnetron sputtering. It was found that the material properties depend strongly on the as-grown layer thickness. Thin AZO films suffer from reduced crystallite size and crystallinity, which is very likely to cause a more pronounced grain boundary scattering effect. As a result, the AZO films become less conductive as the as-grown layer thickness decreases. Electrically, the AZO layer needs to be sufficiently conductive for application as the front electrode of thin-film Si solar cells.

After deposition, these sputtered AZO films were surface textured through a wet-chemical HCl etching process. A sufficient light scattering capability, represented by the transmission haze value, is required for thin-film Si solar cell applications. The haze value of the textured AZO films not only depends on the etching procedure, but is also strongly affected by the initial as-grown layer thickness. The AZO film with as-grown thickness of 900 nm shows a haze value of 22% at 600 nm wavelength after etching for 40 s, which gets reduced to 19% for the 700 nm film and 12% for the 500 nm thick film. Hence, as the front electrode of superstrate thin-film Si solar cells, the AZO layer must be thick enough (>700 nm), to accommodate the thickness reduction during the texturing process,

in order to simultaneously achieve both low electrical resistance and good optical scattering properties.

Acknowledgements

The Solar Energy Research Institute of Singapore (SERIS) is sponsored by the National University of Singapore (NUS) and Singapore's National Research Foundation (NRF) through the Singapore Economic Development Board (EDB). This research was supported by the NRF, Prime Minister's Office, Singapore under its Clean Energy Research Programme (CERP, Award No. NRF2011EWT-CERP001-019). X.Y. acknowledges a PhD scholarship funded by SERIS and the NUS Graduate School for Integrative Sciences and Engineering (NGS) and SERIS.

References

[1] A.V. Shah, H. Schade, M. Vanecek, J. Meier, E. Vallat-Sauvain, N. Wyrsch, U. Kroll, C. Droz, J. Bailat, Prog. Photovoltaics Res. Appl. 12 (2004) 113–142.
[2] A.G. Aberle, Thin Solid Films 517 (2009) 4706–4710.
[3] G. Beaucarne, Adv. Optoelectron. 2007 (2007).
[4] W. Beyer, J. Hüpkes, H. Stiebig, Thin Solid Films 516 (2007) 147–154.
[5] J. Müller, G. Schöpe, O. Kluth, B. Rech, M. Ruske, J. Trube, B. Szyszka, X. Jiang, G. Bräuer, Thin Solid Films 392 (2001) 327–333.
[6] J. Hu, R.G. Gordon, J. Appl. Phys. 71 (1992) 880–890.
[7] R. Groenen, J.L. Linden, H.R.M. van Lierop, D.C. Schram, A.D. Kuypers, M.C.M. van de Sanden, Appl. Surf. Sci. 173 (2001) 40–43.
[8] C. Guillén, J. Herrero, Vacuum 84 (2010) 924–929.
[9] S.-S. Lin, J.-L. Huang, Surf. Coatings Technol. 185 (2004) 222–227.
[10] J. Müller, B. Rech, J. Springer, M. Vanecek, Sol. Energy 77 (2004) 917–930.
[11] J. Hüpkes, S.E. Pust, W. Böttler, A. Gordijn, N. Wyrsch, D. Güttler, A.N. Tiwari, L. Gordon, Y. Qiu, in: Proceedings of 24th European Photovoltaic Solar Energy Conference and Exhibition, 2009, pp. 2766–2769.
[12] Y. Nasuno, M. Kondo, A. Matsuda, in: Proceedings of 28th IEEE Photovoltaic Specialists Conference, 2000, pp. 142–145.
[13] E. Bunte, H. Zhu, J. Hüpkes, J. Owen, EPJ Photovoltaics 2 (2011) 20602.
[14] J.I. Owen, J. Hüpkes, H. Zhu, E. Bunte, S.E. Pust, Phys. Status Solidi A 208 (2011) 109–113.
[15] H. Zhu, J. Hüpkes, E. Bunte, J. Owen, S.M. Huang, Sol. Energy Mater. Sol. Cells 95 (2011) 964–968.
[16] S. Rahmane, M.S. Aida, M.A. Djouadi, N. Barreau, Superlattices Microstruct. 79 (2015) 148–155.
[17] K.H. Ri, Y. Wang, W.L. Zhou, J.X. Gao, X.J. Wang, J. Yu, Appl. Surf. Sci. 258 (2011) 1283–1289.
[18] L. Yuan-dong, W. De-miao, J. Hao, L. Jing-ping, Z. Jian, in: Proceedings of 11th IEEE International Conference on Solid-state and Integrated Circuit Technology, 2012, pp. 1–3.
[19] K.-W. Seo, H.-S. Shin, J.-H. Lee, K.-B. Chung, H.-K. Kim, Vacuum 101 (2014) 250–256.
[20] F.A. Garcés, N. Budini, R.D. Arce, J.A. Schmidt, Thin Solid Films 574 (2015) 162–168.
[21] O. Madani Ghahfarokhi, K. Chakanga, S. Geissendoerfer, O. Sergeev, K. von Maydell, C. Agert, Prog. Photovoltaics Res. Appl. 23 (2014) 1340–1352.
[22] W. Böttler, V. Smirnov, J. Hüpkes, F. Finger, Phys. Status Solidi A 209 (2012) 1144–1149.
[23] V. Smirnov, W. Böttler, J. Hüpkes, F. Finger, Energy Procedia 44 (2014) 223–228.
[24] O. Kluth, G. Schöpe, J. Hüpkes, C. Agashe, J. Müller, B. Rech, Thin Solid Films 442 (2003) 80–85.
[25] X. Yan, S. Venkataraj, A.G. Aberle, Energy Procedia 33 (2013) 157–165.
[26] X. Yan, S. Venkataraj, A.G. Aberle, Int. J. Photoenergy 2015 (2015) 548984.
[27] Standard IEC 60904–3 Ed.2: Measurement Principles for Terrestrial PV Solar Devices with Reference Spectral Irradiance Data, 2008.
[28] B.D. Cullity, S.R. Stock, Elements of X-ray Diffraction, third ed., 2001. Prentice Hall, Upper Saddle River, New Jersey, USA.
[29] H. Stiebig, M. Schulte, C. Zahren, C. Haase, B. Rech, P. Lechner, in: Proceedings of SPIE, 2006, 619701–619701.
[30] S. Venkataraj, J. Wang, P. Vayalakkara, A.G. Aberle, IEEE J. Photovoltaics 3 (2013) 605–612.
[31] J. Wang, S. Venkataraj, C. Battaglia, P. Vayalakkara, A.G. Aberle, Jpn. J. Appl. Phys. 51 (2012) 10NB08.
[32] M. Tadatsugu, Semicond. Sci. Technol. 20 (2005) S35.
[33] F.K. Shan, B.C. Shin, S.W. Jang, Y.S. Yu, J. Eur. Ceram. Soc. 24 (2004) 1015–1018.
[34] K.L. Chopra, S. Major, D.K. Pandya, Thin Solid Films 102 (1983) 1–46.
[35] D. Song, Appl. Surf. Sci. 254 (2008) 4171–4178.
[36] T.C. Damen, S.P.S. Porto, B. Tell, Phys. Rev. 142 (1966) 570–574.
[37] H. Morkoç, Ü. Özgür, Zinc Oxide, Fundamentals, Materials and Device Technology, Wiley VCH, 2009.
[38] C. Charpentier, P. Prod'homme, I. Maurin, M. Chaigneau, P. Roca i Cabarrocas, EPJ Photovoltaics 2 (2011) 25002.
[39] M. Rajalakshmi, A.K. Arora, B.S. Bendre, S. Mahamuni, J. Appl. Phys. 87 (2000) 2445–2448.
[40] S.B. Majumder, M. Jain, P.S. Dobal, R.S. Katiyar, Mater. Sci. Eng. B 103 (2003) 16–25.
[41] S. Fernández, O. de Abril, F.B. Naranjo, J.J. Gandía, Sol. Energy Mater. Sol. Cells 95 (2011) 2281–2286.
[42] W. Lee, T. Hwang, S. Lee, S.-Y. Lee, J. Kang, B. Lee, J. Kim, T. Moon, B. Park, Nano Energy 17 (2015) 180–186.
[43] M. Taeho, Y. Wonki, J. Kwang Sun, A. Seh-Won, L. Sungeun, J. Minho, S. Hui Youn, P. Kyuho, L. Heon-Min, Appl. Phys. Express 3 (2010) 095801.
[44] O. Kluth, B. Rech, L. Houben, S. Wieder, G. Schöpe, C. Beneking, H. Wagner, A. Löffl, H.W. Schock, Thin Solid Films 351 (1999) 247–253.
[45] T. Tohsophon, J. Hüpkes, H. Siekmann, B. Rech, M. Schultheis, N. Sirikulrat, Thin Solid Films 516 (2008) 4628–4632.
[46] J. Hüpkes, J.I. Owen, S.E. Pust, E. Bunte, ChemPhysChem 13 (2012) 66–73.
[47] J.N. Ding, F. Ye, N.Y. Yuan, C.B. Tan, Y.Y. Zhu, G.Q. Ding, Z.H. Chen, Appl. Surf. Sci. 257 (2010) 1420–1424.
[48] J. Hüpkes, J.I. Owen, S.E. Pust, E. Bunte, ChemPhysChem 13 (2012) 66–73.
[49] J. Müller, G. Schöpe, O. Kluth, B. Rech, V. Sittinger, B. Szyszka, R. Geyer, P. Lechner, H. Schade, M. Ruske, G. Dittmar, H.-P. Bochem, Thin Solid Films 442 (2003) 158–162.
[50] H. Zhu, J. Hüpkes, E. Bunte, S.M. Huang, Appl. Surf. Sci. 261 (2012) 268–275.